J Electroceram (2006) 16:263–269
DOI 10.1007/s10832-006-9862-8

Optimisation of interdigitated electrodes for piezoelectric actuators and active fibre composites

C. R. Bowen · L. J. Nelson · R. Stevens · M. G. Cain · M. Stewart

Abstract The optimisation of the interdigitated electrode (IDE) design for active fibre composites was performed using finite element analysis. The effect of the IDE geometry (electrode width and spacing) and electroceramic substrate thickness on the developed strain for bulk PZT substrates was modelled. The modelling results show that the highest strain is generated when the electrode width equals half the substrate thickness and for thin substrates the electrode finger spacing can be reduced to enable lower driving voltages. Approximately 80% of the maximum d_{33} strain can be achieved with an electrode separation to substrate thickness ratio greater than 4. The results present simple coherent guidelines for the optimisation of electrode geometry for piezoelectric actuators and active fibre composites.

Keywords Piezoelectric · Fibre · Composite · Interdigitated · Electrode · Finite element analysis

1 Introduction

Fine scale piezoelectric lead zirconate titanate (PZT) fibres having diameters less than 250 μm are finding uses in ultrasonic transducers [1] and novel geometry composites consisting of PZT fibres with interdigitated surface electrodes [2]. Such composites, as shown in Fig. 1, are commonly referred to as Active Fibre Composites (AFCs) or Macrofibre Composites (MFCs). They have potential for use as actuators and sensors [3], structural health monitoring systems [4] and active/passive vibration damping systems [5]. Considerable effort is underway, developing high performance/strain fibres [6–9]. A significant and additional factor when determining the piezoelectric strain is the geometry of the interdigitaded electrode (IDE) that is used to direct the electric field to in-plane directions, thus taking advantage of the d_{33} mode of actuation. Research on the effect of electrode geometry has been limited [10–12]. In this work finite element analysis is used to enable a greater understanding of factors that influence the strain output, such as electrode finger width, electrode finger separation, and substrate thickness. Model outputs will be presented in a manner that attempts to simplify the choice of the interdigitaded electrode geometry for actuator devices.

C. R. Bowen (✉) · L. J. Nelson · R. Stevens
Materials Research Centre, Department of Mechanical Engineering, University of Bath, Bath, BA2 7AY, UK

M. G. Cain · M. Stewart
National Physical Laboratory, Teddington, Middlesex, TW11 0LW, UK

2 Optimisation of interdigital electrode design

2.1 Electrode modelling

A schematic 2-D representation of an IDE on a bulk PZT substrate is shown in Fig. 2(a), which illustrates the non-uniform electric field lines which are known to result from such an electrode geometry [10–12]. Key parameters associated with the interdigitated electrode geometry are the electrode finger width (w) and electrode finger spacing (s). The electrode substrate thickness (t) has also been shown to influence device performance [10, 11]. The effect of these parameters on the actuation performance of a bulk PZT substrate was modelled using the finite element analysis using the coupled field analysis in ANSYS. The modelled representative volume element (RVE) is highlighted in Fig. 2(a). The expanded and meshed RVE is shown in Fig. 2(b) with appropriate dimensions. The surfaces are numbered in order

Table 1 Boundary conditions of displacement (U) electrical potential (V) and electrical displacement (D) applied to the RVE

Surface number	Mechanical conditions	Electrical conditions
1	Symmetry ($U_x = 0$)	$D_x = 0$
2	Symmetry ($U_y = 0$)	$D_y = 0$
3	U_x coupled	$V = 0V$
4	Free	$V = +V/2$ on electrode, $D_y = 0$ elsewere

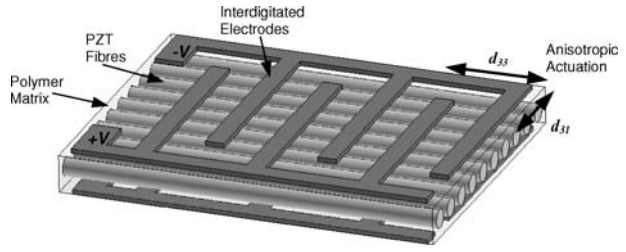

Fig. 1 The construction of the active fibre composite, showing peiezoelectic ceramic fibres, polymer matrix and interdigitated surface electrodes

to define the appropriate boundary conditions for the model; these are shown in Table 1.

The model was constructed in the x-y plane for 2-D modelling. The substrate was defined as a monolithic PZT-5A material and meshed with 2-D coupled-field elements having piezoelectric capability. The element was set to plane strain conditions, implying that the model extends indefinitely in the z-direction. The element mesh size was set to be fine at the electrode edge to capture localised effects. The electrode in Fig. 2(b) was not modelled explicitly, but its presence was captured by the imposed electrical boundary conditions. Appropriate mechanical and electrical boundary conditions are detailed in Table 1.

Previous research [10–12] has shown that the electric field direction within the substrate is non-uniform and will follow the field lines depicted in Fig. 2(a). Since the poling of such IDE devices is performed using the IDEs, the direction of poling will follow these field lines, and the material properties will continuously change with respect to the model axis. In this case, the substrate was considered to be uniformly poled in the x-direction. This simplification should prove adequate for large electrode separations in which the majority of the device response will be attributed to the region between the electrodes, where the material is uniformly poled. However, differences between the modelled and actual response at small electrode separations could exist as a result of this simplification. Beckert and Kreher included an inhomogeneous poling state in ANSYS via a two-step process to examine firstly the electric field distribution (Step 1) which determined the local poling state (Step 2) [12].

Model dimensions were varied to investigate the effect of electrode finger width, electrode finger separation, and substrate thickness. The figure of merit used to assess the electrode geometry effects was chosen as the strain (S) developed in the x-direction per unit applied voltage. Plots of electric field strength in the x-direction at the substrate centre axis ($y = 0$) were also used to gain an insight into the influence of the IDE geometry.

2.2 Results

2.2.1 Electrode width (w)

Our results, showing the effect of electrode width on the developed strain, are presented in Fig. 3. Figure 3(a) shows the strain per unit applied voltage as a function of electrode width for a range of electrode separations. Firstly, as the electrode separation is reduced the strain per unit applied voltage increases. This simply results from a higher electric field for a given voltage and does not necessarily advocate that small electrode separations increase performance, as will be highlighted when the electrode separation (s) results are discussed. More importantly, this figure shows that there exists an optimum width of electrode for which the strain per unit applied voltage is at a maximum, and that this optimum width is independent of electrode separation and substrate thickness. The optimum occurs when the electrode width equals half the substrate thickness ($w/t = 0.5$). Any deviation from this value has a greater effect on the strain at small electrode separations.

To understand the origin of this optimum width it is necessary to examine how the electric field in the substrate is

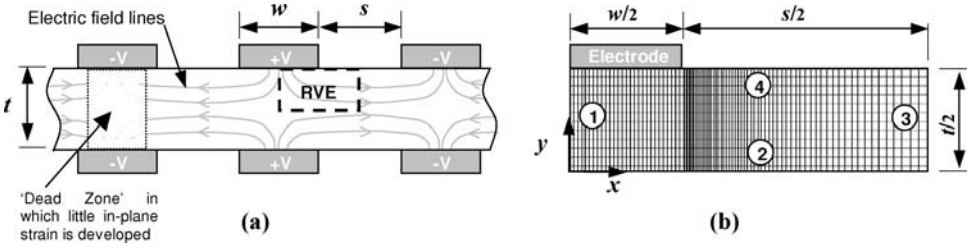

Fig. 2 (a) 2-D interdigitated electrode schematic showing the electric field lines, geometry notation, and representative volume element (RVE). (b) RVE with numbered boundaries, appropriate dimensions and an example of a finite element mesh

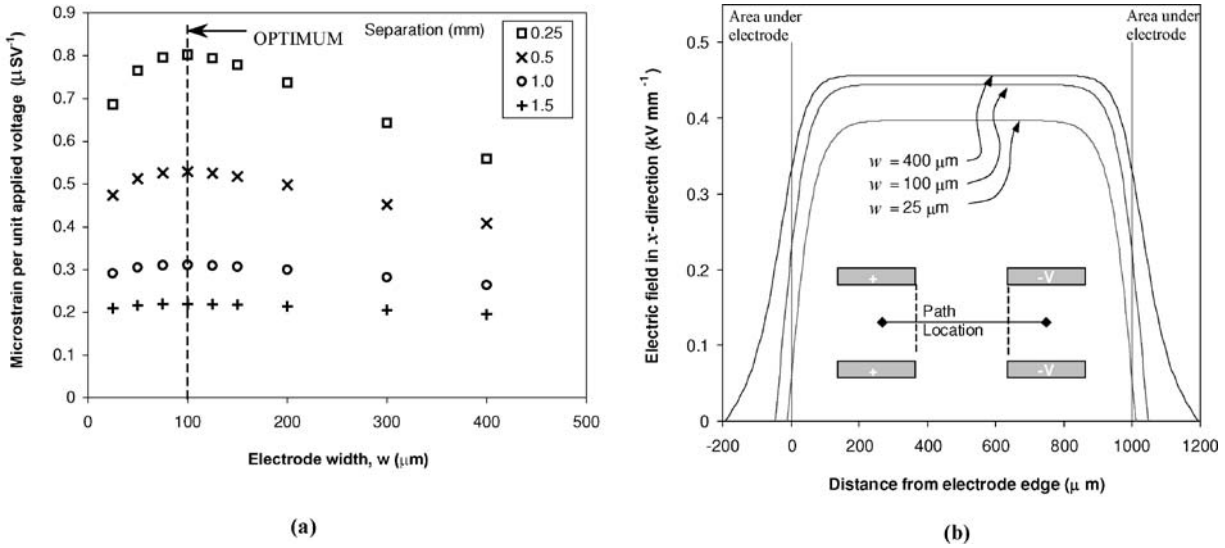

Fig. 3 Finite element results for electrode width analysis showing (a) the effect of electrode width on the strain response of an interdigital electroded PZT substrate ($t = 200\ \mu$m) for four electrode separations, and (b) path plots of electric field in x-direction at the substrate centre axis ($y = 0$) for three electrode widths ($t = 200\ \mu$m, $s = 1$ mm, $V = 0.5$ kV)

affected by the electrode width at constant thickness and separation ($t = 200$ mm, $s = 1$ mm). Figure 3(b) demonstrates the electric field in the poling (x)-direction at the substrate centre axis ($y = 0$) for both the optimum w/t ratio, and for larger and smaller w/t ratios. For wide electrodes ($w = 400\ \mu$m, $w/t = 2$) the electric field strength in the x-direction between the electrodes is increased, but there also exists a high proportion of 'dead area' under the electrode, where the field in the x-direction is relatively low. For thin electrodes ($w = 25\ \mu$m, $w/t = 0.125$) the proportion of dead area is lower, but the electric field in the x-direction is also low. The w/t ratio that induces optimum strain is a balance between the proportion of dead area under the electrode and the strength of electric field in the x-direction between the electrodes. As already stated, this optimum occurs at a w/t ratio of 0.5 ($w = 100\ \mu$m in Fig. 3(b)).

An alternative method of displaying the results of this analysis is in the form of an electric field vector plot. The advantage of this representation over the path plot method is that it allows visualisation of both the magnitude and direction of the electric field within the entire substrate. This reveals important information not available from the path plot method presented previously. Figure 4 shows vector plots of the electric field within the modelled RVE for the three electrode widths presented in Fig. 3(b). The direction of the electric field is denoted by the arrow direction, while the greyscale of the arrow indicates the field strength. The electrode location is indicated by the grey region, on the top surface of each of the substrates.

At large electrode widths, there is a significant dead zone below the electrodes, where the field is perpendicular to the actuation direction (x). For thin electrodes, a relatively weak field is observed between the electrode fingers. In addition to confirming the results of the path plot analysis (Fig. 3(b)), the vector plots presented in Fig. 4 show that a field concentration exists at the electrode edge. The magnitude of the field strength in this location increases as the w/t ratio is reduced, whilst the direction remains largely unaffected. Modelling and actual device studies [10, 13], show that the non-uniform fields present at electrode edges can cause cracking of the piezoelectric substrate resulting in device deterioration. This is a consequence of the large and non-uniform mechanical stresses induced via the piezoelectric effect. Although induced stresses are not quantified in this study, they are an important effect that could lead to device failure. These effects need to be considered in future modelling, which could also investigate the effect of functionally graded fibres, and the influence of polymer layers inserted between the electrode and the piezoelectric fibre. These polymer layers could act as a buffer zone for the field and stress concentration effects, although this would be at the expense of a reduced strain [10, 12].

2.2.2 *Substrate thickness (t)*

With the optimum electrode width determined, and the underlying reasons understood, it is possible to investigate the effect of substrate thickness on the strain output of the device. Results summarising the effect of substrate thickness are presented in Fig. 5. In this analysis, the substrate thickness was varied while the electrode separation and w/t ratio remained constant ($s = 1$ mm, $w/t = 0.5$). Figure 5(a), which plots strain per unit applied voltage versus substrate thickness, highlights that a reduction in the substrate thickness

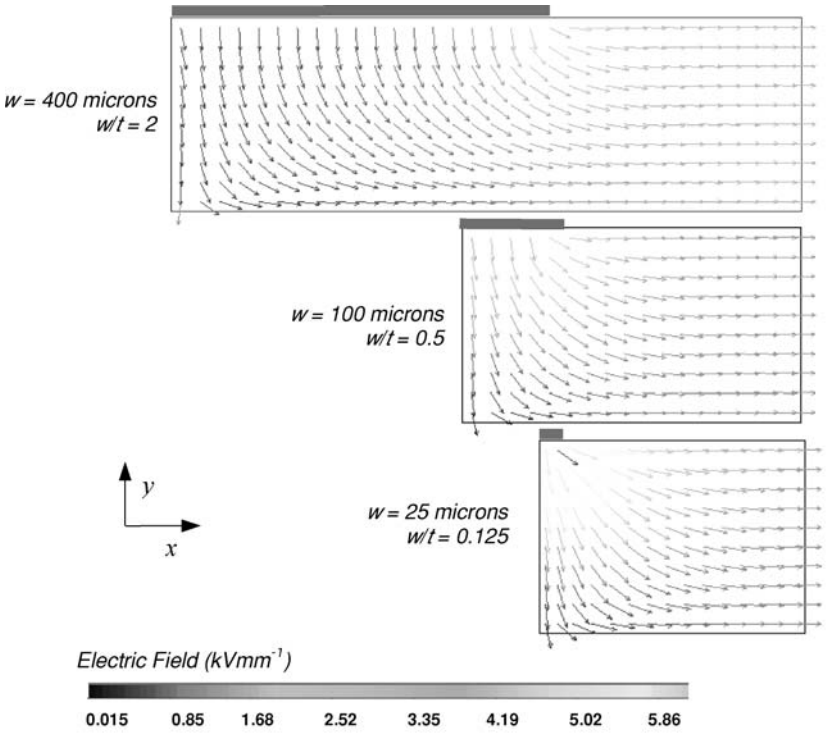

Fig. 4 Vector plots of electric field distribution within the modelled RVE of an IDE structure with varying electrode widths. Voltage = 0.5 kV, PZT thickness = 200 μm, electrode separation = 1.0 mm. The electrode locations are indicated by the light grey region, on the surface of each substrate

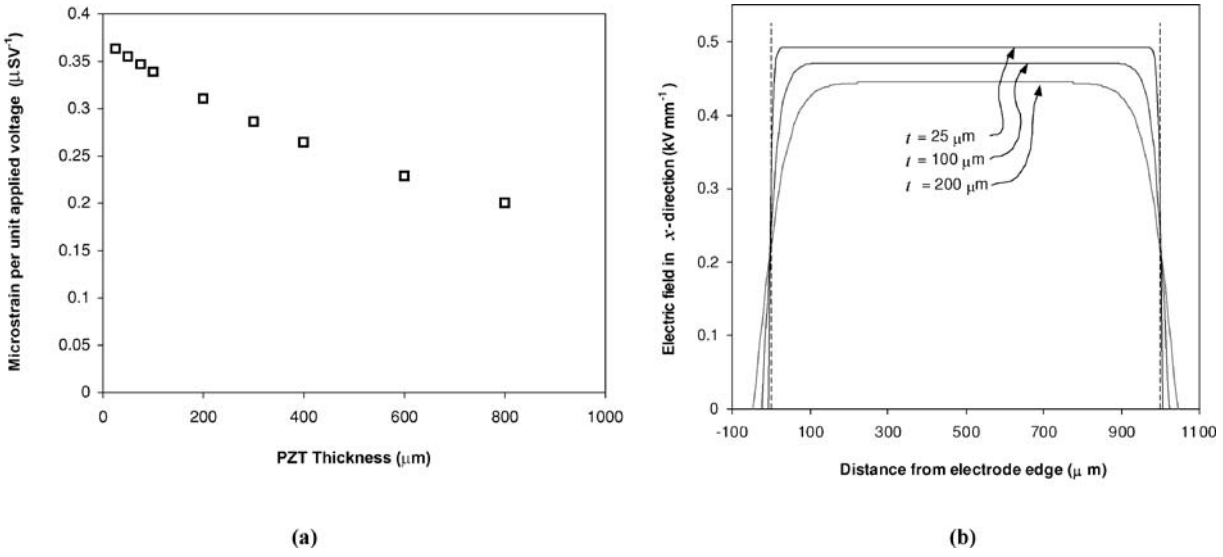

(a) **(b)**

Fig. 5 Finite element results for substrate thickness analysis showing (a) the effect of substrate thickness (for $w/t = 0.5$ and $s = 1$ mm) on the strain response of an interdigital electroded substrate, and (b) Path plots of electric field in x-direction at the substrate centre axis ($y = 0$) for three substrate thicknesses ($w/t = 0.5$, $s = 1$ mm, $V = 0.5$ kV)

increases the strain developed. The reason behind the increased strain is twofold, and can be seen by examination of Fig. 5(b), which shows electric field in the x-direction at the substrate centre axis for three values of substrate thickness. Firstly, as the substrate thickness is reduced the electric field becomes directed into the in-plane direction over a shorter distance, reducing the proportion of 'dead area'. Secondly, as the substrate thickness is reduced, the electric field between the electrodes becomes larger. Both these effects result from the opposing electrodes becoming closer as the substrate thickness is reduced, when they exert a stronger influence on one another. To quantify this effect, a 17% increase in the strain per unit voltage can be expected when the substrate is reduced from a 200 to 25 μm. The results obtained have

shown that thin substrates, and electrodes widths conforming to the optimum *w/t* ratio of 0.5, provide increased actuation performance.

2.2.3 Electrode separation (s)

The final parameter to be examined for optimisation is the electrode finger spacing. It has already been shown that 'dead zones' exist below the electrode fingers, with the field magnitude being low, and out of plane. With large electrode separations the proportion of dead zones is low, but the voltage required to operate the device is high. In contrast, small electrode separations reduce the operational voltage, but increase the proportion of 'dead zone'. There exists a compromise between the achievable actuation strain and operational voltage. Simply plotting the results of actuation strain per unit applied voltage as a function of electrode separation gives little insight into the effects of electrode separation. To gain more from the results it is desirable to quantify how much strain degradation arises from the dead zones. This can be achieved by comparing the FE results to an 'ideal actuator' in which there are no dead zones (all electric field vectors aligned in the in-plane direction). A schematic of the electric field distribution in a true 'IDE actuator', and the desired 'ideal actuator' is presented in Fig. 6

To quantify the degradation in actuation performance, the IDE strain response is compared to an idealised situation in which the field is uniform and aligned in the actuation direction. For a monolithic piezoelectric material electroded on opposite faces separated by a distance s, the strain per unit voltage as a function of electrode separation will obey the relationship in Eq. (1).

$$\frac{S}{V} = \frac{d_{33}}{s} \tag{1}$$

To investigate the effect of electrode separation, a model with a fixed *w/t* ratio, 0.5, was constructed, and the electrode separation was varied from 0.01 to 100 mm. Figure 7 summarises the results obtained. Figure 7(a) shows the strain response as a function of electrode separation for a substrate thickness of 25 μm and contains two data sets, the first is from the finite element analysis and is labelled 'IDE response.' This data shows that decreasing the electrode separation increases the strain per unit voltage; this suggests a small electrode separation is desirable for increased actuation.

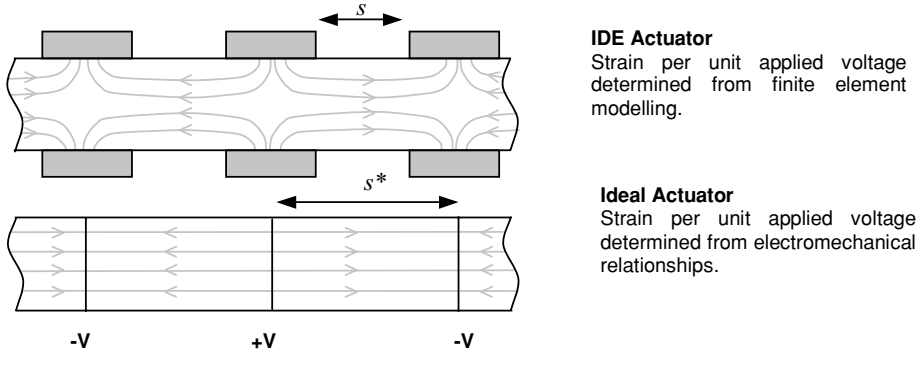

Fig. 6 Schematic representations of the electric field vector for the interdigitaded geometry electrode, and an ideal case with no dead zones

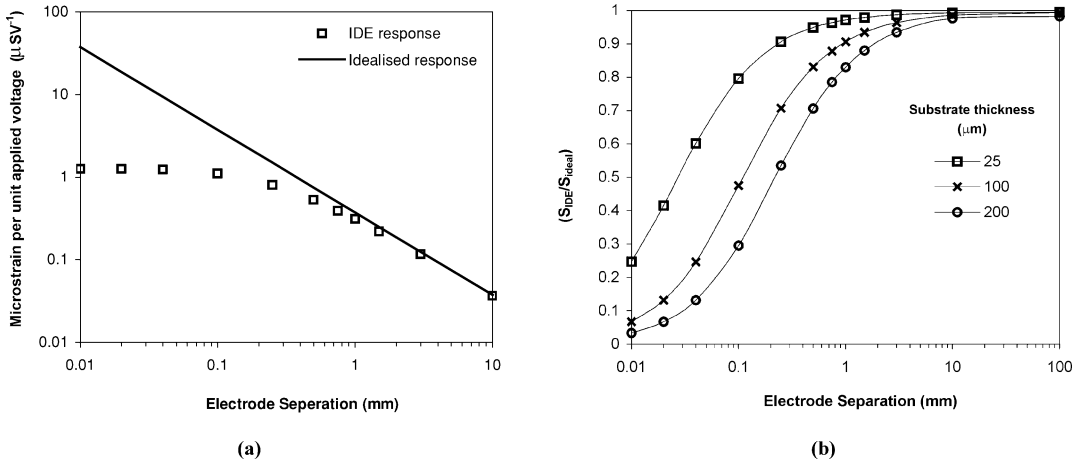

Fig. 7 Results of the electrode separation analysis showing (a) the IDE and idealised strain response as a function of electrode separation, and (b) the strain response of an IDE substrate compared to that of the idealised strain response for three substrate thicknesses

The deviation of the IDE strain S_{IDE}, from ideal response S_{ideal}, can be used to quantify the degradation in actuation resulting from the dead zones directly below the electrode area. This degradation is shown in Fig. 7(b), which plots S_{IDE}/S_{ideal} as a function of electrode separation for three PZT thicknesses. In all cases the electrode width was set so that $w/t = 0.5$. At large electrode separations (>10 mm) the response is close to that of the ideal case. As the electrode separation is reduced the dead zones begin to dominate the response, and the IDE strain starts to diminish compared to the idealised response. Since a primary reason for using an IDE is to take advantage of the d_{33} response, which is approximately twice as large as the d_{31} response, once the reduction in actuation is greater than 50%, this benefit is lost. From Fig. 7(b) it is apparent that for thinner substrates the electrode separation can be reduced significantly while still maintaining a high proportion of the optimum d_{33} response.

The extension of this work to fibre-matrix substrates used for active fibre composites (Fig. 1) implies small diameter fibres are required to enable production of thin substrates. Thus manufacturing techniques have not only to be capable of producing high quality fibres, but also small diameters fibres. The graph presented in Fig. 7(b) can be used as a design guide for IDEs. For example, to obtain at least 80% of the d_{33} response, electrode separations must satisfy $s/t > 4$. Using this guideline, substrates with a thickness of 200 μm require electrode separations greater than 0.8 mm. This separation reduces to 0.1 mm for a substrate thickness of 25 μm. This is significant result since a reduced electrode separation enables lower driving voltages to be used, which at present are typically very high. A clear benefit from using thin substrates (small diameter fibres in AFCs) now becomes apparent. Thus manufacturing techniques for fibres must be capable of producing high quality smaller diameter fibres, along with close control over IDE geometry.

3 Conclusions

Modelling of the interdidgitated electrode structure on a PZT substrate has given an insight into how the strain response is affected by electrode width, substrate thickness and electrode finger separation. The optimum strain was found to occur at an electrode width to substrate thickness (w/t) ratio of 0.5. A reduction in the substrate thickness has been shown to increase the strain output of the device by reducing 'dead areas' and increasing the field level between the electrode fingers. Finally, it was shown that 80% of the maximum d_{33} strain can be achieved with an electrode separation to substrate thickness (s/t) ratio greater than 4. This has important implications since thin substrates allow smaller electrode separations, allowing large reductions in the operational voltage. As a result of these findings it becomes clear that fibre manufacturing techniques have not only to be capable of producing high quality fibres, but also fibres with small diameters. The data presented provides simple design guidelines for IDE patterns on piezoelectric actuators and active fibre composites.

Material property data

Table 2 Material property data for PZT-5A [14] used for the finite element analysis

Material property	Value
e_{33}	15.8 Cm^{-1}
e_{31}	-5.2 Cm^{-1}
e_{15}	12.3 Cm^{-1}
$\varepsilon_{33}^{T/\varepsilon_0}$	1700
$\varepsilon_{11}^{T/\varepsilon_0}$	1730
c_{11}^{E}	12.0×10^{10} Pa
c_{12}^{E}	7.52×10^{10} Pa
c_{13}^{E}	7.51×10^{10} Pa
c_{33}^{E}	11.1×10^{10} Pa
c_{44}^{E}	2.1×10^{10} Pa

Acknowledgment The authors would like to acknowledge NPL and the University of Bath for funding this research.

References

1. R.J. Meyer, T. R. Shrout, and S. Yoshikawa, "Development of ultrafine scale piezoelectric fibers for the use in high frequency 1-3 transducers," in *Proc. 10th IEEE Int. Symp. On Applications of Ferroelectrics*, edited by B.M. Kulwicki et al. (IEEE, New York, 1996), p. 547.
2. L.J. Nelson, "Smart piezoelectric fibre composites," *Materials Science and Technology*, **18**, 1245 (2002).
3. A. Schonecker, U. Keitel, W. Kreher, D. Sporn, W. Watazka, and K. Pannkoke, *Ferroelectrics*, **224**, 435 (1999).
4. M.J. Schulz, M.J. Sundaresan, A. Ghoshal, and P.F. Pai, "Active fiber composites for structural health monitoring," in *Proc. of SPIE*, edited by C.S. Lynch (SPIE, Bellingham USA, 2000), vol. 3992, pp. 13–24.
5. S. Yoshikawa, U. Selvaraj, K.G. Brooks, and S.K. Kurtz, "Piezoelectric PZT tubes and fibres for passive vibration damping," in *Proc. 8th IEEE Int. Symp. on Applications of Ferroelectrics*, edited by M. Liu et al. (IEEE, New York, 1992), pp. 269–272.
6. H.B. Strock, M.R. Pascucci, M.V. Parish, A.A. Bent, and T.R. Shrout, "Active PZT fibers, a commercial production process," in *Proc. of SPIE*, edited by W. Wuttig (SPIE, Wellingham USA, 1999), vol. 3675, pp. 22–31.
7. R. Meyer, T. Shrout, and S. Yoshikawa, *J. Am. Ceram. Soc.*, **81**, 861 (1998).
8. J.D. French and R.B. Cass, *Am. Ceram. Soc. Bull.*, **77**, 61 (1998).
9. F. Meister, D. Vorbach, F.Niemz, T. Schulze, and E. Taeger, *Materialwiss. Werkst.*, **34**, 262 (2003).

10. D.J. Warkentin, "Modeling and electrode optimisation for torsional IDE piezoceramics," in 'Smart Structures and Materials 2000: Smart Structures and Intergrated Systems,' in *Proc. of SPIE*, edited by N.M. Werely (SPIE, Belingham USA, 2000), vol. 3985, pp. 840–854.
11. N. Hagood, R. Kindel, K. Ghandi, and P. Gaudenzi, "Improving transverse actuation of piezoceramics using interdigitated surface electrodes," in *Proc. of SPIE*, edited by N.W. Hagood (SPIE Bellingham USA, 1993), vol. 1917, pp. 341–352.
12. W. Beckert and W.S. Kreher, *Comp. Mat. Sci*., **26**, 36 (2003).
13. C.R. Bowen, A. Bowles, S. Drake, N. Johnson, and S. Mahon, *Ferroelectrics*, **228**, 257 (1999).
14. D. Berlincourt, H.H.A. Krueger, and C. Near, "Properties of piezoelectric ceramics," Technical Publication TP = 226, Morgan Electroceramics (Jan. 2002).